Proton Sensing of CLC-0 Mutant E166D

Sonia Traverso, Giovanni Zifarelli, Rita Aiello, and Michael Pusch

Istituto di Biofisica, Consiglio Nazionale delle Ricerche, I-16149 Genova, Italy

CLC Cl^- channels are homodimers in which each subunit has a proper pore and a (fast) gate. An additional slow gate acts on both pores. A conserved glutamate (E166 in CLC-0) is a major determinant of gating in CLC-0 and is crucially involved in Cl^-/H^+ antiport of CLC-ec1, a CLC of known structure. We constructed tandem dimers with one wild-type (WT) and one mutant subunit (E166A or E166D) to show that these mutations of E166 specifically alter the fast gate of the pore to which they belong without effect on the fast gate of the neighboring pore. In addition both mutations activate the common slow gate. E166A pores have a large, voltage-independent open probability of the fast gate (p_{open}), whereas p_{open} of E166D pores is dramatically reduced. Similar to WT, p_{open} of E166D was increased by lowering pH_{int}. At negative voltages, E166D presents a persistent inward current that is blocked by *p*-chlorophenoxy-acetic acid (CPA) and increased at low pH_{ext}. The pH_{ext} dependence of the persistent current is analogous to a similar steady inward current in WT CLC-0. Surprisingly, however, the underlying unitary conductance of the persistent current in E166D is about an order of magnitude smaller than that of the transient deactivating inward Cl^- current. Collectively, our data support the possibility that the mutated CLC-0 channel E166D can assume two distinct open states. Voltage-independent protonation of D166 from the outside favors a low conductance state, whereas protonation from the inside favors the high conductance state.

The Journal of General Physiology

INTRODUCTION

CLC proteins are a multigene family present in all phyla (Jentsch et al., 2005). The founding member, called CLC-0, was identified as a voltage-dependent Cl^- channel in the electric organ of *Torpedo californica* (White and Miller, 1979; Miller and White, 1980). After the cloning of CLC-0 (Jentsch et al., 1990), homologues were found in many prokaryotes and all eukaryotes. The physiological importance of CLC proteins is underscored by their involvement in several human genetic diseases and the surprising phenotypes of knockout models (Jentsch et al., 2005; Uchida and Sasaki, 2005). Functions of CLC proteins range from the regulation of the skeletal muscle membrane potential to transepithelial transport and pH homeostasis of intracellular organelles (Jentsch et al., 2005; Pusch and Jentsch, 2005). From the recent X-ray structure of bacterial CLCs it is now clear that CLC proteins contain two identical subunits in which each subunit presents an independent pathway for Cl^- ions (Dutzler et al., 2002, 2003). Such a "double-barreled" architecture had been conjectured by Miller and colleagues early on from the single channel behavior of the *Torpedo* channel (Miller and White, 1984) and it was also predicted from later mutagenesis work and a lower resolution structure (Ludewig et al., 1996; Middleton et al., 1996; Mindell et al., 2001). The homodimeric structure enables two mechanisms of gating: a fast gate acting on each pore independently and a slow gate acting on both pores simultaneously (Miller and White, 1984). The fast gate of each pore of CLC-0 opens and closes in the time range of milliseconds, whereas the slow gate opens and closes both pores simultaneously in the time range of seconds to minutes (Pusch et al., 1997). While the mechanism of the slow gate is still obscure, the X-ray structure of CLC-ec1 allowed important insights into the mechanism of the fast gate of CLC-0. Each subunit of CLC-ec1 contains 18 α helices that wrap around a central part, the putative pore in which three ion binding sites are present (S_{int}, S_{cent}, and S_{ext}) (Dutzler et al., 2002, 2003). In the bacterial protein CLC-ec1, S_{ext} is occupied by the side chain of the glutamate carboxylate group of residue E148, which is probably negatively charged (Dutzler et al., 2002). This side chain appeared to block the movement of Cl^- ions toward the extracellular side, and the structure of the WT protein was therefore assumed to represent a closed pore (Dutzler et al., 2002). In accordance with this hypothesis, in the structure of CLC-ec1 in which the glutamate was mutated to an alanine (E148A), a chloride ion was resolved where the E148 side chain is localized in the WT, whereas the remaining structure was almost unaltered (Dutzler et al., 2003). The interpretation of this mutated structure as an open state was supported by the functional results performed in parallel on CLC-0, which showed that the equivalent mutant in CLC-0 (E166A) had an "open," voltage-independent phenotype (Dutzler et al., 2003). This

Correspondence to Michael Pusch: pusch@ge.ibf.cnr.it

Abbreviations used in this paper: CPA, *p*-chlorophenoxy-acetic acid; WT, wild type.

straightforward correlation of the structure of the bacterial CLC-ec1 and the function of the vertebrate CLC-0 is also in agreement with other studies that suggest a structural conservation of CLC proteins (Estévez et al., 2003; Lin and Chen, 2003). However, other studies suggested that the fast gating of CLC-0 involves an additional rearrangement of the intracellular part that is not revealed by the crystal structure of E148A (Accardi and Pusch, 2003; Traverso et al., 2003). In fact, the functional equivalence of CLC-0 and CLC-ec1 was challenged when Accardi and Miller demonstrated that CLC-ec1 is actually not a Cl^- ion channel but an electrogenic Cl^-/H^+ antiporter with an apparent stoichiometry of 2 Cl^-:1 H^+ (Accardi and Miller, 2004). Moreover it has been recently shown that also mammalian proteins of the same family, CLC-3, CLC-4, and CLC-5, exhibit Cl^-/H^+ antiporter activity (Picollo and Pusch, 2005; Scheel et al., 2005). In contrast, CLC-0 is clearly an ion channel with well-defined, relatively large single channel events (Hanke and Miller, 1983; Bauer et al., 1991) and Nernstian dependence of the reversal potential on the chloride concentration.

The molecular mechanism of transport of CLC-ec1 and CLC-3–5 is not understood and it is currently unclear how the gating and permeation properties of CLC-0 are correlated to it. It seems, however, likely that the proton dependence of the fast gate of CLC-0 is somehow related to the Cl^-/H^+ antiport of CLC-ec1. For example, extracellular acidification opens CLC-0 (Chen and Chen, 2001; Dutzler et al., 2003), probably by protonating E166, mimicking the effect of mutating E166 to a neutral amino acid (Dutzler et al., 2003). The analogous mutations of CLC-ec1 (E148A) and CLC-5 (E211A) abolish H^+ transport (Accardi and Miller, 2004; Picollo and Pusch, 2005; Scheel et al., 2005). Also intracellular acidification strongly activates CLC-0 (Hanke and Miller, 1983) and similarly CLC-1 (Rychkov et al., 1996) by apparently shifting the activation curve to negative voltages.

To better understand the role of protons in the mechanism of protopore gating of CLC-0 we mutated the critical glutamate 166 to the similar amino acid aspartate. Despite the small difference between these two amino acids (one extra CH_2 group in the side chain of glutamate) the kinetics of the WT and of the mutant are very different (Traverso et al., 2003). In the present work, we show that indeed both mutants, E166A and E166D, have a drastically altered protopore gate. However, both mutations, despite their disparate effect on the fast gate, appear to eliminate slow gating processes, locking the slow gate open. We then varied pH_{int} and pH_{ext} and compared the effects on E166D with those described for WT CLC-0. In contrast with what would be expected from the behavior of WT CLC-0, extracellular pH had no effect on E166D outward currents but affected only a persistent inward current present at negative voltages, a current that appears to represent a different conductance state of the channel. Decreasing intracellular pH drastically increased the p_{open} of the channel in a manner that suggests that the protonation from the inside represents one of the major voltage-dependent steps in the opening of the fast gate.

MATERIALS AND METHODS

Molecular Biology and Heterologous Expression

Mutations were introduced by recombinant PCR as previously described (Accardi et al., 2001). Tandem dimers (WT-ED, ED-WT, WT-EA, and EA-WT) were generated as previously described (Ludewig et al., 1996). In brief, the stop codon of the NH_2-terminal subunit was replaced with an SpeI and a KpnI restriction site. The same sites were introduced before the start codon of the COOH-terminal subunit. The Spe I site was used to link both subunits. The linker sequence consisted of four amino acids (G-T-T-S). All constructs were in the PTLN vector (Lorenz et al., 1996). cRNA was transcribed and injected in *Xenopus* oocytes as previously described (Accardi and Pusch, 2000).

Electrophysiology

Currents were recorded using the two-electrode voltage-clamp method and excised patch-clamp recording as previously described (Pusch et al., 2000). For whole oocyte voltage clamp measurements, the bath solution contained (in mM) 100 NaCl (or 100 NaI), 4 $MgSO_4$, 5 HEPES, pH 7.3, and the holding potential was chosen close to the resting membrane potential (-30 to -50 mV). For patch clamping, the intracellular solution contained (in mM): 100 NMDG-Cl, 2 $MgCl_2$, 10 HEPES, 2 EGTA, pH 7.2, whereas the standard extracellular solution contained 100 NMDG-Cl, 5 $MgCl_2$, 10 HEPES, pH 7.2. In both solutions HEPES was substituted by MES for solutions with $5 < pH < 6.5$, bis-Tris-propane for solutions with $pH > 7.8$, and glutamate for solutions with $pH < 5$. Experiments shown in the figures were performed using regular pH of 7.2 for the extracellular solution (for patch-clamp and voltage-clamp recordings) and the intracellular solution (for patch-clamp recordings) unless otherwise noted.

All substances were purchased from Sigma-Aldrich. Solutions in patch-clamp experiments were changed by inserting the patch pipette into perfusion tubes of ~0.5 mm diameter. Patch-clamp data were recorded using an EPC-7 amplifier (HEKA) and the Pulse acquisition program (HEKA) or a custom acquisition program (GePulse) (the acquisition program is available at http://www.ge.cnr.it/ICB/conti_moran_pusch/programs-pusch/software-mik.htm).

The holding potential in patch clamp measurements was 0 mV. Voltage clamp measurements employed an NPI-TEC 05 amplifier (NPI Electronics), and were performed as described previously (Traverso et al., 2003).

Capacity Subtraction

For all (macroscopic) patch-clamp experiments, the capacitive transients were subtracted offline in the following manner. All pulse protocols contained a final pulse to 0 mV with a duration equal or superior to the longest segment of the voltage-clamp pulse protocol. Since at 0 mV (very close to the reversal potential) no ionic current is expected to flow, the current response reflects only the capacitive transient. This response, after appropriate scaling, was used for the subtraction of the capacitive transients at the other test potentials.

Single Channel Analysis

Single channel recordings were generally filtered at 1 kHz or 500 Hz. For the construction of amplitude histograms a bin width of 5 fA was used. Amplitude histograms were fitted with the sum of Gaussian functions, G_i, one for each peak, i,

$$H(I) = \sum_i G_i(I) = \sum_i \frac{a_i}{\sigma_i} \exp\left(-\frac{(I-\mu_i)^2}{2\sigma_i^2}\right),$$

where each Gaussian function is characterized by a mean μ_i, a width σ_i, and amplitude a_i. The relative area, A_i, that is occupied by each Gaussian component was calculated by

$$A_i = \frac{a_i}{\sum_j a_j}$$

and was taken as a measure of the probability to dwell in the conductance state associated with mean μ_i.

Nonstationary Noise Analysis

Nonstationary noise analysis was performed essentially as described earlier (Pusch et al., 1994). In brief, a test pulse was repeatedly applied, and the variance was calculated from the squared difference of consecutive current responses. For the variance-mean analysis, the current range was subdivided into a certain number of bins for a clearer graphical representation. Background variance was measured at the baseline (at 0 mV) and subtracted. The variance-mean plots were fitted with Eq. 1 (see below) with two free parameters, the single channel current i, and the number of channels, N. All primary data analysis was performed with the custom analysis program downloadable at http://www.ge.cnr.it/ICB/conti_moran_pusch/programs-pusch/software-mik.htm. Figures were prepared with SigmaPlot (SPSS Inc.).

pH Measurements

We measured the extracellular pH close to the oocyte surface with a pH-sensitive microelectrode as described by Picollo and Pusch (2005). In brief, silanized (with dichlorodimethylsilane; Sigma-Aldrich) microelectrodes were filled with proton ionophore B (Fluka) and then with a solution containing (in mM) 150 NaCl, 23 NaOH, 40 KH_2PO_4, pH 6.8. Pipettes were connected to a custom built high impedance ($>10^{15}$ Ohm) amplifier and responded with a slope of 57–63 mV per pH unit. The pH-sensitive microelectrodes were gently pushed against the vitelline membrane without penetrating the oocyte. The pH-related signal was recorded as a second input channel in parallel to the membrane current. The extracellular solution for pH measurements contained 100 mM NaCl, 4 mM $MgCl_2$, 0.1 mM HEPES, pH 6.4.

RESULTS

Noise Analysis of Mutant E166D Reveals a Slightly Reduced Conductance

We analyzed mutations of the glutamate E166 of CLC-0 to aspartate (ED) and alanine (EA). Mutating E166 in CLC-0 to alanine leads to an almost constitutively open channel (Dutzler et al., 2003; Traverso et al., 2003), whereas E166D slows down opening at positive potentials and increases the rate of closure at negative potentials (Traverso et al., 2003). In addition, mutant E166D consistently expressed much less current than WT CLC-0 or mutant E166A. In fact, in order to keep currents at a manageable magnitude that could be measured with the two electrode voltage clamp, <1 ng of cRNA was injected for CLC-0, and currents were measured after 1–2 d. In contrast, ~20 ng had to be injected for mutant E166D, and oocytes had to be incubated for at least 3 d to achieve a sizable current (unpublished data). To find out whether a reduced single channel conductance of E166D was responsible for the smaller currents we performed nonstationary noise analysis (Fig. 1). This method provides a good order-of-magnitude estimate of the single channel current and may allow the determination of the absolute open probability (Heinemann and Conti, 1992). Fig. 1 A shows the mean of 80 traces obtained each by stepping the voltage from 0 to 120 mV in an inside-out patch. Fig. 1 B shows the corresponding variance trace, whereas in Fig. 1 C the variance is plotted versus the mean (symbols) together with a fit (line) of the equation

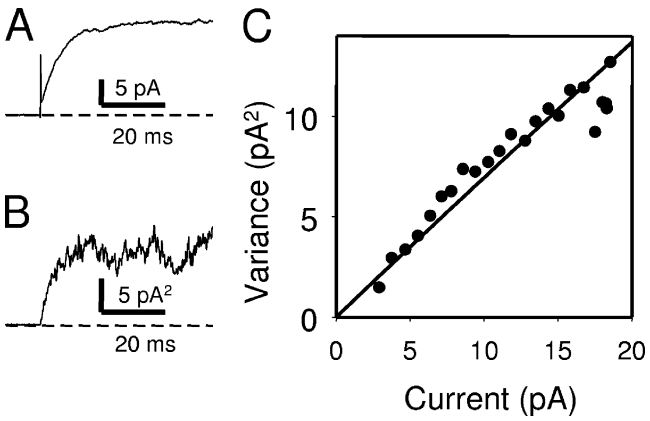

Figure 1. Nonstationary noise analysis of mutant E166D at 120 mV. The figure shows the results from a typical inside-out patch containing many E166D channels. Currents were repeatedly activated at 120 mV (activation time constant ~6 ms) and the mean was calculated (A). The variance was calculated from the mean square difference of consecutive records (Heinemann and Conti, 1992) (B). In C the variance (binned) is plotted versus the mean current (symbols) together with a fit of Eq. 1 (line) with the particular parameters i = 0.70 pA, N = 10^3.

$$\sigma^2 = i*I - I^2/N, \quad (1)$$

where σ^2 is the variance, I the macroscopic current, i the single channel current, and N the number of channels. The average single-channel current obtained from noise analysis at 120 mV was 0.55 ± 0.14 pA (mean ± SD, $n = 6$). Assuming a linear single-channel i-V, this corresponds to a conductance of 4.6 pS. This value is only ~35% smaller than the conductance of WT CLC-0 (~7 pS) (Accardi and Pusch, 2003) and this reduction can thus not explain the small macroscopic currents of mutant E166D. From the nonstationary noise analysis it was not possible to obtain a reliable es-

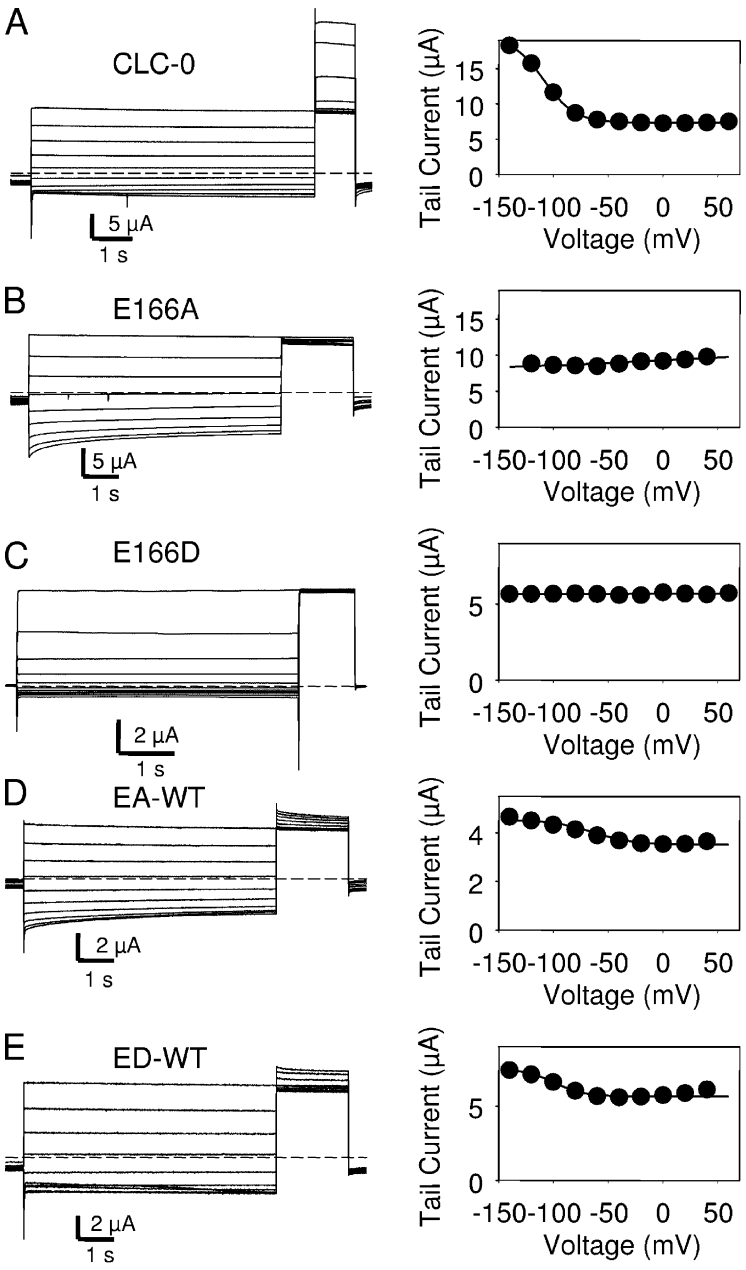

Figure 2. Slow gate of WT, mutants of E166, and heterodimers. Representative recordings are for each construct as indicated in the figure. The left panels show voltage-clamp traces evoked by a standard "slow-gate" protocol (Pusch et al., 1997) that monitors the degree of activation by the variable prepulse at a constant tail pulse of 40 mV. The voltage dependence is shown in the right panels together with fits to a Boltzmann curve with offset. Note that mutants E166A and E166D do not show any voltage dependence of the slow gate, whereas the heterodimers partially recover a voltage-dependent component. Similar results were observed in at least three oocytes for each construct.

timate for the number of channels, and consequently of the absolute open probability, because the variance-mean plots showed little curvature. This indicates that the maximal open probability is significantly smaller than 0.5, as is indeed the case (see below).

Tandem Mutant-WT and WT Mutant Dimers Differentiate Effects on Fast and Slow Gate

The next question we asked was: In what specific manner do mutations E166A and E166D affect the fast (protopore) gate and the slow (common) gate? The slow gate of CLC-0 is voltage dependent with activation favored at negative voltages (Miller and Richard, 1990; Pusch et al., 1997) (Fig. 2 A). No hyperpolarization activation could be detected for either E166A (Fig. 2 B) or E166D (Fig. 2 C). A further hint that the slow gate is locked open in mutant E166D was obtained from the study of the double mutant E166D/C212S that includes the mutation C212S, that locks open the slow gate of CLC-0 (Lin et al., 1999). The double mutant E166D/C212S had properties indistinguishable from the single mutant E166D (unpublished data). These results indicate that the slow gate is either locked open or rendered voltage independent by both mutations E166A and E166D.

We next made four tandem dimeric constructs consisting of one WT and one mutant subunit: WT-ED, WT-EA, ED-WT, and EA-WT. For example, the notation WT-

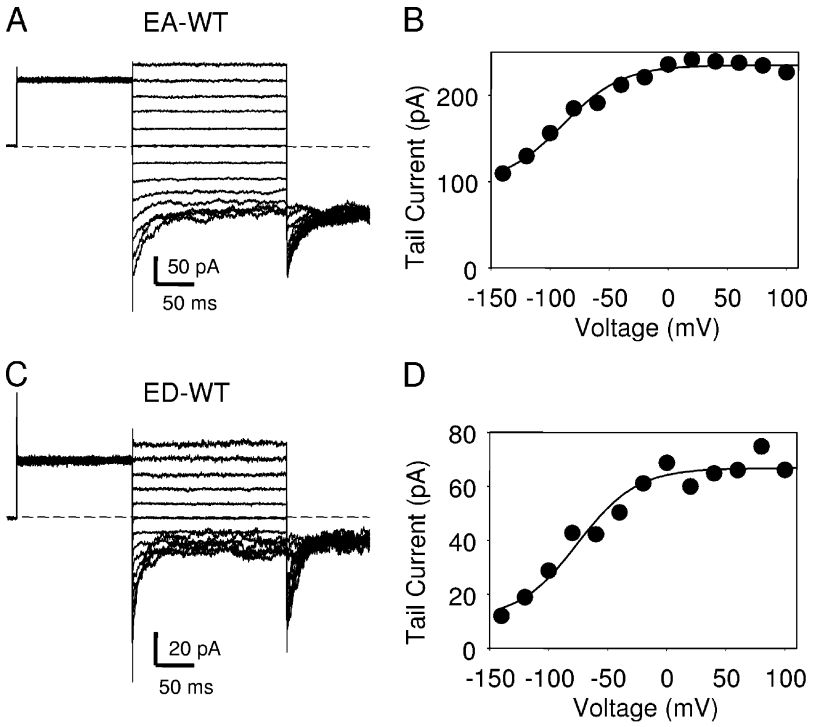

Figure 3. Fast gate of heterodimers. Representative inside-out patch recordings are shown for the EA-WT (A) and the ED-WT (B) dimer. The degree of activation of the fast gate is monitored as the initial current at the constant −140 mV tail pulse, plotted as absolute values in B and D, respectively. The solid lines in B and D represent fits of the equation $I(V) = I_{max}\ (p_{min} + (1 - p_{min})/(1 + \exp((V - V_{1/2})/k)))$ with the parameters $p_{min} = 0.42$, $V_{1/2} = -89$ mV, $k = 25$ mV for EA-WT; and $p_{min} = 0.16$, $V_{1/2} = -75$ mV, $k = 25$ mV for ED-WT. The $p_{open}(V)$ curve of the EA-WT dimer is very similar to that described for WT CLC-0 under identical conditions (Accardi and Pusch, 2003). Similar results were obtained in at least three patches for each kind of tandem dimer.

ED indicates that the first subunit is WT and the second bears the E166D mutation. No difference could be observed between heterodimers with opposite order (i.e., ED-WT versus WT-ED and EA-WT versus WT-EA) (unpublished data). All dimeric constructs, including a control WT-WT dimer, expressed similar levels of current (conductance ranged between 50 and 200 μS after 1 d of incubation), suggesting that the E166D mutation has no (dominant) effect on protein processing or stability. However, we cannot completely rule out that mutation E166D alters protein trafficking.

Interestingly, all dimeric constructs partially recovered a voltage dependence of the slow gate (Fig. 2, D and E). The fact that the slow gate was only partially recovered demonstrates that for all dimeric constructs, both subunits contribute to channel gating. Macroscopic currents of EA-WT dimers on a faster time scale from inside-out patches are shown in Fig. 3 A. The voltage dependence of the fast gate, plotted in Fig. 3 B, differs from that of WT CLC-0 mainly by an increased offset at negative voltages, reflecting probably the voltage-independent contribution of the E166A pores. This interpretation was further confirmed by single channel analysis.

Fig. 4 A shows a single channel trace of the dimer EA-WT at −100 mV. For most of the time the channel behaves as the superposition of a WT pore and a pore, of similar conductance, that is almost always open. Occasionally, currents reach the baseline (indicated by arrows in Fig. 4 A). These events probably represent longer closures of the "EA pore." A similar behavior has been also previously observed in homomeric E166A channels (Traverso et al., 2003). These closures are not closures of the slow gate because the neighboring "WT pore" continues to open and close. Whether these slow transitions of the EA pore reflect "residual" fast gate transitions remains to be studied. An amplitude histogram over a stretch without such long closures (see bracket with * in Fig. 4 A) yielded a p_{open} of 0.64 of the fluctuating pore (Fig. 4 C), relatively close to the WT p_{open} at −100 mV (p_{open}[WT] ∼ 0.75; Accardi and Pusch, 2003). This strongly suggests that indeed the fast fluctuating conductance level represents the WT pore whereas the long open times correspond to the EA pore, demonstrating that the mutation strongly affects the fast protopore gate, without affecting the fast gate of the neighboring WT pore.

The fast gate properties of the ED-WT resemble those of homodimeric WT CLC-0 as illustrated in Fig. 3 (C and D). The same holds true for WT-ED dimers (unpublished data). In particular, at positive voltage, no slowly activating component similar to that seen in Fig. 1 is visible in patch or voltage-clamp recordings from dimers containing E166D. Thus, there seems to be no contribution of the ED subunit to the "heterodimeric" ED/WT currents, even though we know from the slow-gate recovery, that the ED subunit is present in the dimer. This might be caused by a very small open probability of the fast gate of mutant E166D as suggested by the noise analysis described above. To directly test this hypothesis we measured single ED-WT channels. The advantage of using the dimer instead of measuring directly single E166D channels is that the presence of

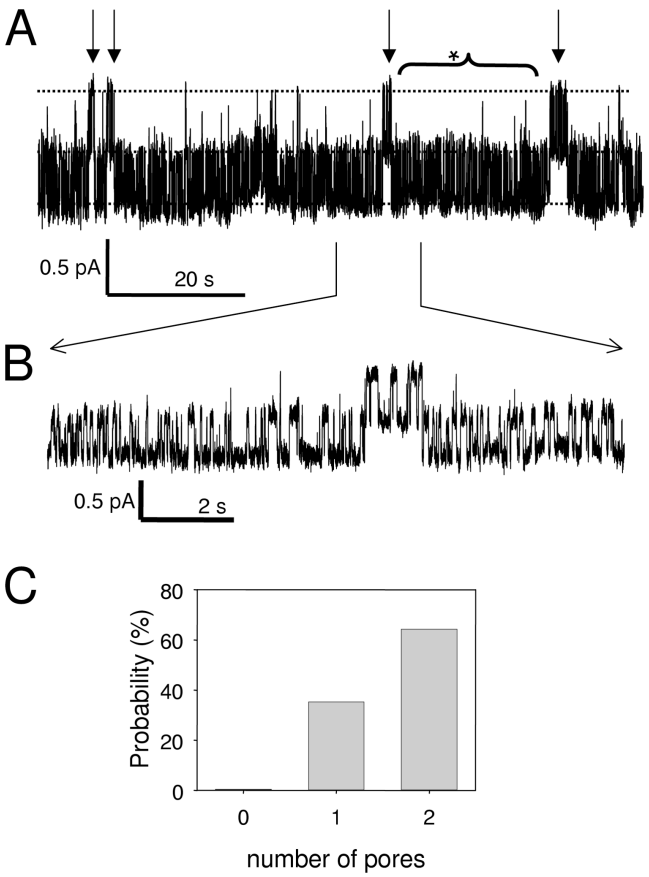

Figure 4. Single channel phenotype of EA-WT dimer. In A, a recording at −100 mV of a patch containing a single EA-WT dimer is shown. Three conductance levels can be seen (dashed lines) corresponding to the baseline (both pores closed), one pore open, and two pores open. The behavior can be well described by the superposition of a WT pore with relatively fast gating and a p_{open} around 0.64 and a pore that is mostly open with occasional longer closures (see arrows in A). The fast gating is better seen in B, which shows part of the upper trace at an expanded time scale. C shows the relative areas obtained by fitting the sum of three Gaussian functions to the amplitude histogram obtained over the stretch marked with the bracket with asterisk in A. In this period, no long closure event is seen and the area of the level 2 peak is 64% of the total area whereas the baseline peak is <1%. Similar results were seen in a total of four single-channel patches (one patch WT-EA, three patches EA-WT).

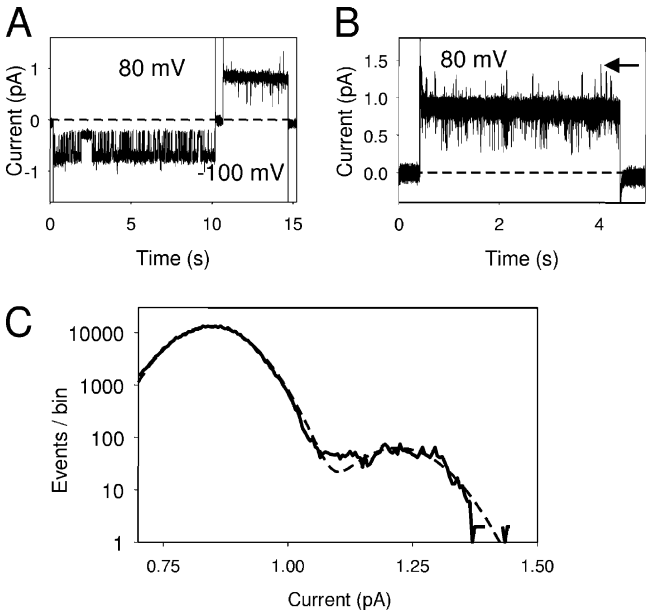

Figure 5. Phenotype of dimer WT-ED. In A, a current trace recorded from a patch with a single WT-ED dimer is shown. The voltage was stepped from 0 to −100 mV, back to 0 mV for a brief time and then to 80 mV. Currents appear almost like a single WT pore at −100 mV (with a $p_{open} \sim 0.7$) and at 80 mV with a p_{open} of almost 1. However, brief openings to a second open level are visible at 80 mV. To visualize the "spikes" at 80 mV, B shows the superposition of 10 consecutive records at an expanded time scale showing only the pulse to 80 mV. To quantify the p_{open} of the ED pore on top of the WT pore at 80 mV, the amplitude histogram of all records at 80 mV was constructed and limited to the part I > 0.7 pA (C, solid line). In this way, interferences from short closures were eliminated. The amplitude histogram was fitted by the sum of two Gaussian functions (dashed line in C). Since the p_{open} of the WT pore is close to one, the relative area of the higher peak directly reflects the p_{open} of the ED pore. In this case it amounts to 0.51%. Similar results were seen in a total of six single-channel patches (two patches WT-ED, four patches ED-WT)

only one channel in the patch can be assured by the presence of a single WT-like pore. Indeed, single channel events of WT-ED dimers almost behaved as if they consisted of an isolated single WT pore. This is illustrated in Fig. 5 A, which shows a recording of a patch subjected to voltage pulses to first −100 mV and then +80 mV. At −100 mV, a single pore switches between open and closed states, with an apparent open probability ($p \sim 0.77$) close to that of the fast gate of CLC-0 at this voltage (p_{open}[WT] ∼ 0.75; Accardi and Pusch, 2003). At +80 mV, the pore is almost permanently open, which is consistent with the high open probability of the fast gate of CLC-0 at this voltage. However, closer inspection of several traces recorded at 80 mV (Fig. 5 B) reveals rare short openings to a higher conductance level (see arrow in Fig. 5 B). Also many brief interruptions to the baseline can be seen, representing probably brief closures of the WT fast gate. In fact, the expected mean closed time of the WT fast gate is given by $1/\alpha$ (where α is the opening rate) being ∼0.3 ms at 80 mV, which we calculated using the known parameters for WT (Chen and Miller, 1996, Eq. 9 and Table II) together with the external chloride concentration used in our experiments. To quantify the contribution of the openings to the second open conductance level (arrow in Fig. 5 B) to the overall current, we constructed an amplitude histogram on a logarithmic scale with I > 0.7 pA, excluding thus the brief closure events. Fitting the histogram with the sum of two Gaussian functions (Fig. 5 C) results in an estimate of a contribution of ∼0.5% of the small peak at ∼1.3 pA to the overall cur-

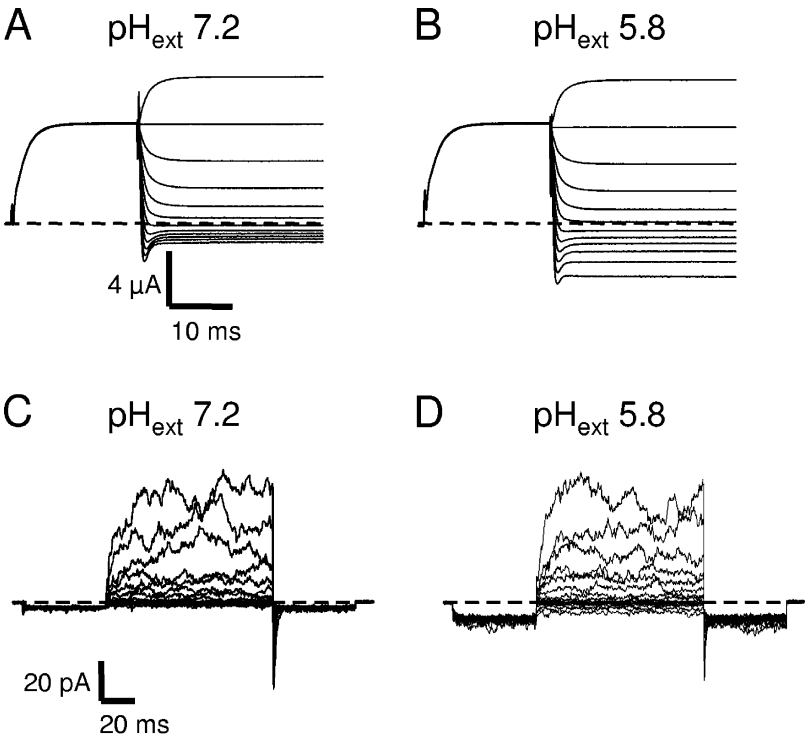

Figure 6. Dependence of E166D on the extracellular pH. (A and B) Two-electrode voltage clamp recordings from the same oocyte at pH_{ext} 7.2 (A) and pH_{ext} 5.8 (B). The pulse protocol consisted of a prepulse to 60 mV followed by pulse to a variable voltage (from 80 to −140 mV). (C and D) Recordings from an outside out patch perfused with an extracellular solution at pH 7.2 (C) and 5.8 (D). The pulse protocol consisted of a prepulse to −140 mV followed by pulse to a variable voltage (from 160 to −140 mV) and a final tail pulse to −140 mV.

rent. Given that the open probability of the fast gate of WT is practically one at 80 mV, this contribution directly reflects the open probability of the fast gate of E166D if the openings are interpreted as arising from an E166D pore. The conductance of the putative ED pore estimated from the histogram analysis at 80 mV (∼4.7 pS) is very similar to that obtained from the nonstationary noise analysis at 120 mV (∼4.6 pS), consistent with this interpretation of the single-channel results. Thus, the almost complete lack of an obvious contribution of E166D pores to macroscopic and single channel currents in WT/ED heteromers probably arises from the very small open probability of E166D pores even at 80 mV.

Collectively, results from macroscopic and single channel current measurements show that both E166 mutations (E166A and E166D) strongly affect the fast gate, without influence on the fast gate of the neighbor subunit, and that the conservative mutation E166D leads to a drastic reduction of the open probability of the fast gate.

Dependence of E166D on Extracellular pH

Having established that E166D strongly alters the fast gate, our next purpose was to analyze the effects of different extracellular and intracellular pH on this mutant and compare it to the published effects on WT CLC-0. In two-electrode voltage clamp measurements we varied pH_{ext} from 5.8 to 8.3. WT CLC-0 is strongly activated by a reduction of pH_{ext} (Chen and Chen, 2001; Dutzler et al., 2003). Given that the open probability of E166D is very small (see above and below), we expected that its p_{open} would be strongly augmented at low extracellular pH. Surprisingly, almost no change of E166D currents were observed at positive voltages, and only the inward currents at negative voltages were significantly enhanced (Fig. 6, A and B). The latter phenomenon was studied in further detail using outside-out patches. Changing pH_{ext} from 7.2 to 5.8 in outside-out patches outward currents were almost unchanged, whereas we observed a significant increase of the steady-state inward current present at −140 mV (Fig. 6, C and D). This current is not a leak current as it is blocked by *p*-chlorophenoxy-acetic acid (CPA) (see below, Fig. 9 A). A more detailed investigation of its properties is presented below.

Dependence of E166D on Intracellular pH

In contrast to pH_{ext}, pH_{int} had a drastic effect on the currents carried by mutant E166D. In Fig. 7 A, currents measured from the same inside-out patch are shown at different pH_{int} (pH 7.2, pH 6.8, pH 6.3, and pH 5.8). These currents were elicited by pulses up to 220 mV and channel activation was monitored by a tail pulse to −140 mV. Currents are clearly activated by low pH_{int}. This can be seen directly from the current measured at the variable test voltages. But also the initial current at the constant tail pulse to −140 mV is clearly increased at low pH up to 5.3 (Fig. 7 A, insets). A qualitatively different behavior was seen when the pH was further lowered down to 4.3. Fig. 7 B shows current traces from a different inside-out patch at pH_{int} 7.2, 5.8, 4.8, and 4.3.

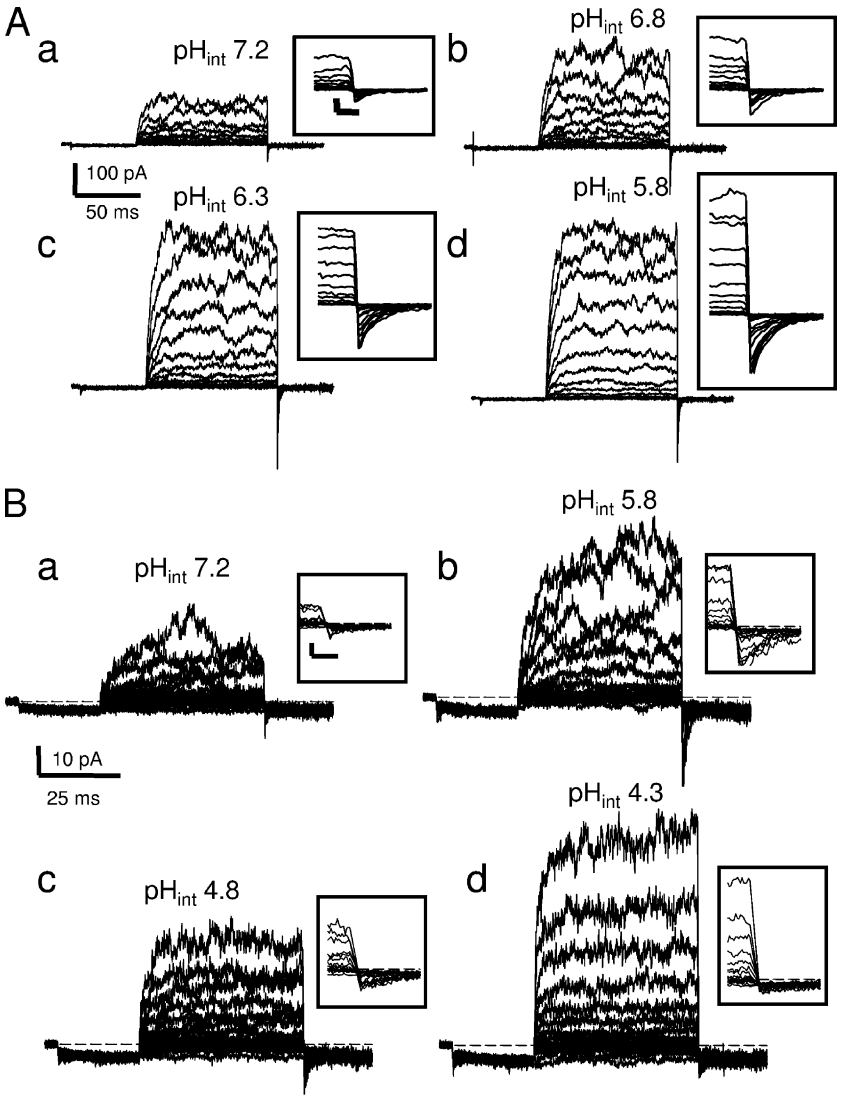

Figure 7. Dependence of E166D on the intracellular pH. (A) Families of current traces recorded from the same inside-out patch at the indicated pH_{int} values. The pulse protocol consisted of a prepulse to −140 mV followed by pulse to a variable voltage (from 220 to −140 mV) and a final tail pulse to −140 mV that served to estimate the open probability as explained in the text. The boxed insets show on a magnified time scale the initial phase of the deactivation at the final tail pulse to −140 mV (horizontal scale bar in inset, 1 ms; vertical scale bar, 30 pA; all insets are drawn at the same scale). Experiments from a different patch are shown in B at the indicated pH_{int} values (scale bars in inset, 1 ms and 10 pA, respectively). Voltage pulses in B were from 180 to −140 mV.

Surprisingly, currents at pH_{int} 4.8 were smaller than currents at pH_{int} 5.8 but increased again at pH_{int} 4.3. Most importantly, the tail currents at the fixed tail voltage of −140 mV were significantly smaller at pH_{int} 4.8 and even smaller at pH_{int} 4.3 compared with pH_{int} 5.8 (Fig. 7 B, insets). Thus, reducing pH_{int} has a biphasic effect on tail current amplitude of mutant E166D: tail currents increase up to pH ∼5.3 and then decrease again. In fact, the tail currents at $pH_{int} < 5.3$ were too small to allow a quantitative analysis. We noted also that it took several minutes to reach a steady-state current level after perfusing patches with $pH_{int} < 5.3$, and also recovery after washing with the control solution was much slower than the speed of the solution exchange. Because of these complications we restricted the quantitative analysis of the effect of pH_{int} on the open probability to values $pH_{int} > 5$. For the quantitative analysis we assumed that the initial current at the constant final "tail" pulse is proportional to the p_{open} at the end of the prepulse to V_p. In Fig. 8 A the normalized initial tail currents are plotted versus V_p. Currents were normalized to the maximum response seen in the same patch for voltages ≥200 mV and pH ≤5.8. This normalization is justified because curves saturated at high voltages at low pH_{int}. The normalization implicitly assumes that the single-channel current at −140 mV is not influenced by pH_{int}. In principle, this is a reasonable assumption because intracellular H^+ are expected to be pushed away from the pore at these negative voltages. For $pH_{int} > 5$, the assumption seems to be justified also by the data, whereas for more acidic pH, tail currents decrease in an apparently paradoxical manner (Fig. 7 B). For $pH_{int} > 5$ the I-V curves were fitted by

$$p(V) = p_{min} + (1 - p_{min})/(1 + \exp((V - V_{1/2})/k)), \quad (2)$$

where the parameter p_{min} accounts for possible leak current and the persistent inward current carried by E166D. The fits resulted in estimates of the voltage of half-maximal activation, $V_{1/2}$, as a function of pH_{int}

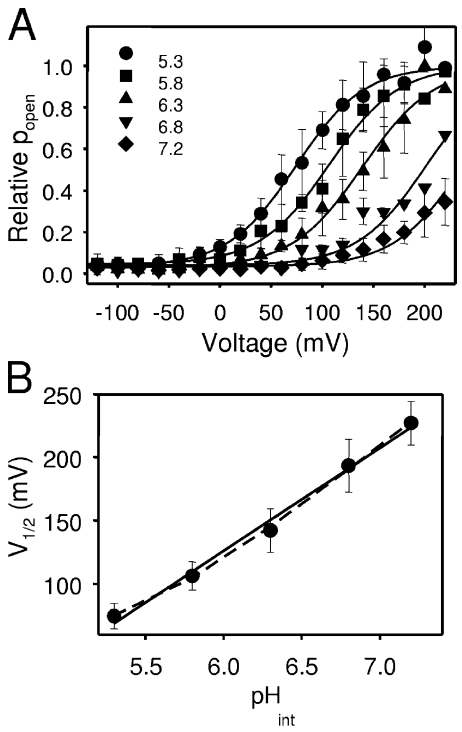

Figure 8. Analysis of the pH_{int} dependence of E166D for pH > 5. (A) Averaged relative p_{open} obtained from the tail currents as explained in the text are plotted versus voltage for each pH_{int} with symbols as indicated. Error bars indicate SD. The solid lines represent fits of Eq. 2. The "slope" parameter, k, was ~33 mV for pH_{int} 5.3, 5.6, and 6.3, whereas it was manually fixed to 34 mV for pH_{int} 6.8 and 7.2. (B) Average $V_{1/2}$ values obtained from fits of the individual experiments plotted versus the respective pH_{int} value (error bars are SD). The solid line is a linear fit with a slope of 81 mV per pH unit. The dashed line is a fit of Eq. 5 resulting in $K_l(0) = 4.3*10^{-8}$, $pK_O = 12.2$, $pK_C = 5.3$, z = 0.59.

(Fig. 8 B). Overall it can be concluded that E166D is dramatically activated by intracellular protons. The $p_{open}(V)$ curve is shifted by ~81 mV per pH unit (see solid line in Fig. 8 B). Assuming that the maximal p_{open} achieved at high voltages and low pH_{int} is close to unity, allows to estimate the absolute p_{open} at all other voltages and pH values. For example at pH_{int} 7.2 and V = 80 mV a p_{open} of 0.95% is estimated (neglecting p_{min} that accounts for possible leak current and the persistent inward current). This is relatively close to the value estimated from the single channel analysis of ED-WT heterodimers (0.5%, see above). However, it has to be kept in mind that the assumption that the open probability approaches one at saturating voltages is probably not fully justified (see Discussion). The low p_{open} at physiological pH values inferred from these measurements and from the single channel analysis most likely explains the small macroscopic current amplitude in voltage clamp experiments. As can be seen in the insets in Fig. 7 A, pH_{int} affects also the kinetics of deactivation: deactivation is slightly faster at high pH_{int}.

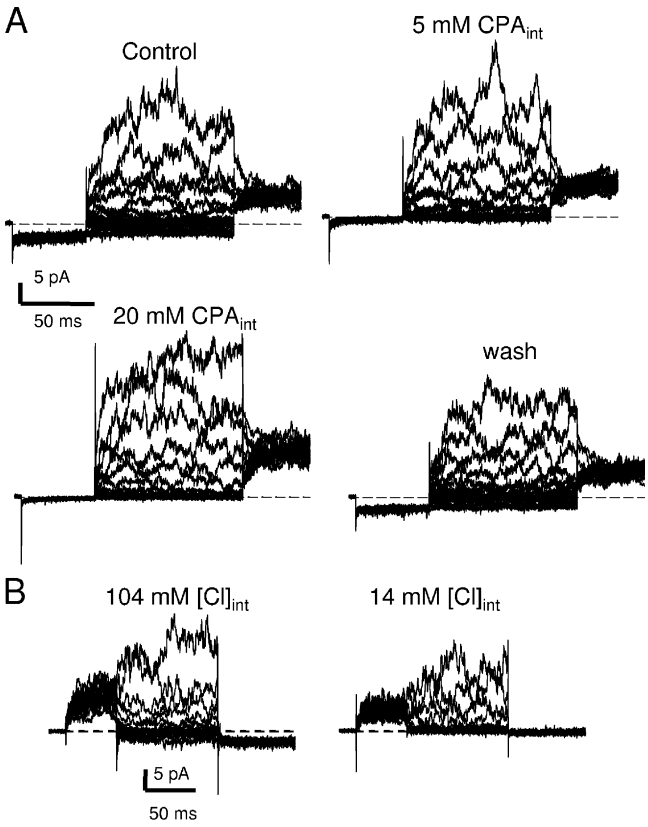

Figure 9. Proof of specificity of the persistent inward current. (A) Currents recorded from an inside-out patch containing many E166D channels in control, in the presence of 5 and 20 mM CPA in the intracellular solution and after washout. The pulse protocol consisted of a prepulse to −140 mV, a variable pulse to voltages from −140 to 160 mV and a constant tail pulse to 100 mV. Note the block of inward currents by CPA. The slight increase of outward currents by CPA was observed consistently, but was not analyzed in detail. (B) Current traces from an inside-out patch with 104 mM Cl^- inside (left) and 14 mM Cl^- inside (right). Intracellular and extracellular pH had standard values in these experiments.

The Persistent Inward Current Is Possibly Mediated by a Different Open State

We characterized the properties of the persistent inward currents at −140 mV in more detail. First, to assure that it is not an unspecific leak current, we applied 5 and 20 mM intracellular CPA, a known blocker of CLC-0 (Accardi and Pusch, 2003; Estévez et al., 2003). Most of the persistent inward current is indeed blocked by 5 mM CPA and practically all inward current is blocked by 20 mM CPA, in a reversible manner (Fig. 9 A). Since the size of the inward current strictly correlated with the size of the outward current (unpublished data), this result shows that the current is carried by E166D proteins and is not an artifact. A further proof of the specificity of the persistent inward current was obtained by reducing intracellular chloride: reducing $[Cl^-]_{int}$ to 14 mM abolished the persistent inward current almost completely (Fig. 9 B).

In noise analysis experiments such as that shown in Fig. 1, we noted that the persistent inward current was associated with a surprisingly small variance. To study this in detail we applied high-resolution nonstationary noise analysis to the deactivating and steady-state part of the current at −140 mV under various conditions. Fig. 10 shows examples performed at various values of pH_{ext}. Data are from different inside-out patches at the indicated pH values. In each case at least 50% of the persistent current at −140 mV was blocked by the application of 5 mM CPA to the intracellular side of the patch showing that the current is not caused by leak (unpublished data). Clearly, at pH_{ext} 6.4, and even more so at pH_{ext} 5.4, the persistent current is much larger relative to the transient inward current (Fig. 10, A–C, a). Actually, at pH_{ext} 5.4, the inward current at −140 mV is practically exclusively composed of an activating component without a transient deactivating component. In each case, the variance associated with the persistent current was very small (Fig. 10, A–C, b). In the subpanels c (Fig. 10, A–C) the variance of the current during the pulse to −140 mV is plotted versus the absolute value of the corresponding mean current, after appropriate binning (circles). For pH_{ext} 7.2, the data are reasonably fitted by Eq. 1 (Fig. 10 A, c, solid line). However, the data are better fitted by a straight line with slope 0.8 pA, that does not cross the origin (Fig. 10 A, c, dashed line; overlaps with data points). At pH_{ext} 6.4 (Fig. 10 B) it is obvious that the data cannot be well fitted by Eq. 1 because the variance is close to zero at steady state even though the current is substantial (Fig. 10 B, c, solid line). The dashed line in Fig. 10 B, c, that fits the data well, has a slope of ∼1 pA. This shows that the transient, deactivating response of E166D at −140 mV is associated with an elementary current of ∼1 pA, corresponding to a single-channel conductance of ∼7 pS. Assuming that the persistent current is carried by ion channel activity, the small variance of the steady-state current could be due to a small unitary conductance or a larger unitary conductance associated with a close-to unity open probability. However, since the persistent current is mediated by E166D proteins, very many of which must be present in the patch illustrated in Fig. 10 to generate the sizeable outward current at 120 mV, the latter possibility can be excluded: a close-to unity open probability together with a conductance similar to that estimated for the transient inward current would generate a much larger inward current than observed. We can therefore conclude that the elementary conductance of the persistent inward current is small. To estimate the elementary current of the steady-state component we use the equation

$$\sigma^2 = i*I*(1-p), \qquad (3)$$

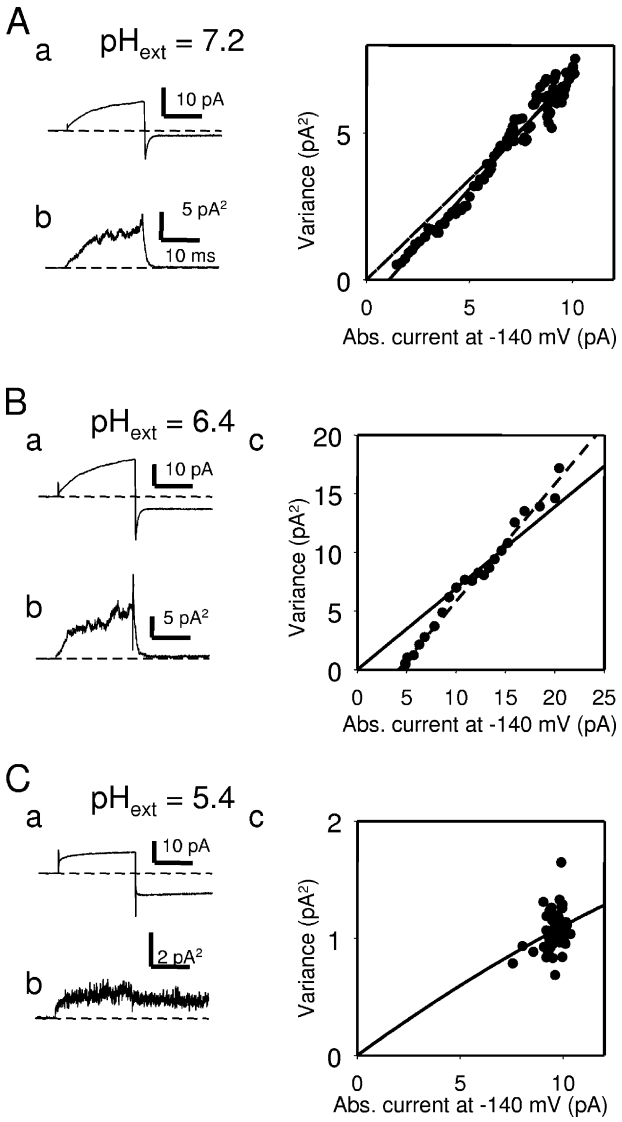

Figure 10. Small unitary conductance underlying the persistent current. In each box (A–C) are shown the results of a nonstationary noise analysis conducted with an inside-out patch with the indicated pH_{ext} values. In each case, subpanel a shows the mean current response from >60 stimulations evoked by a step from 0 to 160 mV and then to −140 mV. Subpanel b shows the corresponding baseline-subtracted variance. Subpanel c shows the plot of the binned variance versus the absolute value of the mean for the segment of the records at −140 mV. Solid lines are best fits of Eq. 1 with i = 0.68 pA (A), i = 0.7 pA (B), i = 0.13 pA (C). The number of channels was very large in A and B, and N = 583 in C. The dashed lines in A and B are linear fits with slopes of 0.79 pA (A) and 1 pA (B) and a current offset of 1.1 pA (A) and 4.2 pA (B). The residual variance at the end of the −140 mV pulse was 0.46 pA^2 in B.

and assuming for simplicity a small open probability $i = \sigma^2/I$. From the measured values of the persistent current, I, and the associated variance, σ^2, an elementary current of ∼0.11 pA at pH_{ext} 6.4 can be calculated, about 10-fold smaller than the elementary current asso-

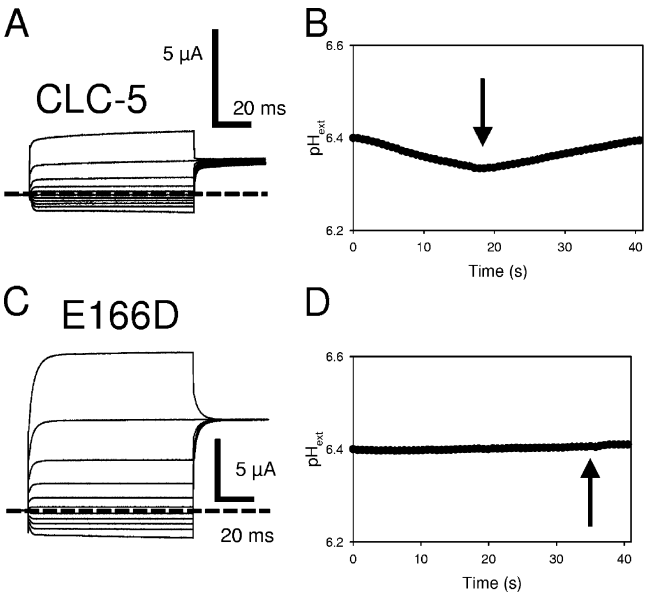

Figure 11. Persistent inward current is not associated with H^+ inward movement. The extracellular pH was measured with a pH-sensitive microelectrode close to the oocyte surface as described in MATERIALS AND METHODS. Currents recorded from a CLC-5–expressing oocyte are shown in A (pulses are from −120 to 80 mV with a constant "tail" pulse to 60 mV). In B, the pH response, shown as a function of time, was evoked by a train of 300-ms pulses to 60 mV (current at 60 mV is ∼1.8 μA) with a 300-ms holding period between the pulses at −20 mV. The arrow indicates the switch off of the voltage clamp, nulling the current and leading to a recovery of pH_{ext}. (C and D) Results from a similar experiment from an oocyte from the same batch expressing mutant E166D. The train of 300-ms pulses was delivered to −100 mV (V_{hold} = −30 mV), where a current of ∼−2 μA was measured. No significant pH change could be detected in >10 oocytes with large expression of E166D, whereas a pH change was robustly detected in all CLC-5–expressing oocytes.

ciated with the transient component (similar results were obtained in more than five patches).

At pH_{ext} 5.4, data are reasonably well fitted with Eq. 1, resulting in an estimate of i = 0.13 pA (Fig. 10 C, c), very similar to the above estimate for the elementary current associated with the persistent current at pH_{ext} 6.4.

Collectively, the noise analysis demonstrates that the persistent inward current is carried by a different mechanism, of lower elementary conductance, than the transient inward current or the slowly activating outward current. It likely represents either a different open state or a transport mode instead of a channel mode.

The Persistent Inward Current Is Not Associated with H^+ Transport

It might be hypothesized that the persistent inward current reflects Cl^-/H^+ antiport. This would explain the marked dependence on pH_{ext} and the small variance. To test for this we measured the extracellular pH close to the oocyte surface using a pH-sensitive microelectrode in a solution of low buffer capacity (0.1 mM HEPES) and a slightly acidic pH of 6.4 to increase the magnitude of the inward current. To assay for H^+ transport we applied a train of pulses to negative voltages (between −100 and −140 mV). In CLC-5–expressing oocytes, tested at positive voltages in the same solution and at similar current levels (Fig. 11 A), a robust change of the extracellular pH could be recorded (Fig. 11 B; Picollo and Pusch, 2005). Since inward currents generated by mutant E166D are relatively small (e.g., Fig. 6), we used only oocytes that expressed currents >12 μA at 80 mV for this analysis (Fig. 11 C). However, even in such highly expressing oocytes, no significant increase of the extracellular pH close to the oocyte surface could be detected (Fig. 11 D). This result suggests that the persistent inward current is not mediated to a large extent by protons.

DISCUSSION

The recent discovery that CLC-ec1 is not a Cl^- channel but a Cl^-/H^+ antiporter induced us to investigate better the role of protons in gating of CLC-0. Dutzler et al. (2003) have shown that a major element that is responsible for CLC gating is the glutamate residue E166. Mutating it to alanine, glutamine, or serine leads to a complete loss of voltage and chloride dependence of gating of CLC-0 (Dutzler et al., 2003; Traverso et al., 2003) with channels appearing almost permanently open. X-ray crystallographical analysis of the equivalent mutations of the bacterial CLC-ec1 (E148A, E148Q) beautifully revealed that the location of the presumably negatively charged side chain of E148 in the WT structure was occupied by a Cl^- ion in the mutant structures (Dutzler et al., 2003). Accardi and Miller found that the Cl^-/H^+ antiport activity of CLC-ec1 was abolished by the mutation E148A and that it behaves like a passive Cl^--selective channel or uniporter (Accardi and Miller, 2004). These results indicate that there is an intimate relationship between gating of CLC-0 and Cl^-/H^+ antiport of CLC-ec1. A Cl^-/H^+ antiport function was recently described also for the mammalian proteins CLC-4 and CLC-5 (Scheel et al., 2005; Picollo and Pusch, 2005), demonstrating that the function of the bacterial proteins is of far greater relevance to human physiology than previously thought.

In the present work we sought to obtain more insight into the relationship between gating and H^+ transport by analyzing in detail the properties of an interesting mutation of the glutamate E166 in CLC-0; a mutation into the very similar amino acid aspartate. Aspartate differs from glutamate only by the lack of one CH_2 group while the acidic properties of the two side chains are quite similar (pK_{Asp} ∼3.9, pK_{Glut} ∼4.1; Fersht, 1998). Despite this small structural difference, the mutant

E166D has drastic effects on gating. E166D slows down opening at positive potentials (Traverso et al., 2003), increases the rate of closure to negative potentials, and has a very low open probability at physiological pH and voltages <100 mV. Our first aim was to understand whether this drastically different gating of E166D (and E166A) was due to a specific alteration of the fast gate or of the slow gate. From the published single channel data of the mutant E166A (Dutzler et al., 2003; Traverso et al., 2003) it was clear that the fast gating transitions were abolished in the mutant E166A. However, no single channel data were available for E166D. Interestingly, we found here that both mutations (E166A and E166D) appear to lock the slow gate in an open state, similar to the C212S mutation (Lin et al., 1999). Slow-gate closing was partially recovered in tandem heterodimers containing one mutant and one WT subunit. The mechanism of the slow gate and its relationship with the fast gate, however, remain an enigma.

Based on single-channel analysis of dimeric constructs containing one WT and one mutant subunit, we could definitely conclude that in addition to their effect on the slow gate, both mutants strongly alter the fast gate. E166A strongly increases the open probability and renders it insensitive to voltage and chloride concentration, whereas E166D strongly reduces p_{open}. An effect of these mutations on the fast gate might seem almost trivial since the glutamate side chain is directly "occluding" the individual "protopores" in the WT CLC-ec1 structure (Dutzler et al., 2002). However, mutating only one amino acid upstream of E166 in CLC-0, namely K165 into arginine, a mutation that leads to a strong inwardly rectifying phenotype (Ludewig et al., 1997), drastically affects mainly the slow gate, rendering it much faster in a manner that the overall macroscopic gating relaxations are reflecting mostly slow gate transitions (unpublished data), with little direct effect on the fast gate.

In addition, the dimeric ED-WT (and WT-ED) constructs allowed us to determine the absolute open probability of the fast gate of the ED pore. This was not possible using nonstationary noise analysis, because this method fails if the p_{open} is significantly smaller than 0.5. It turned out that at 80 mV the fast gate of E166D pores has a p_{open} of <0.01, whereas WT CLC-0 has a maximal p_{open} of 1 at this voltage. It would have been practically almost impossible to determine such a low p_{open} using direct single channel recording of ED homomers because of the difficulty in determining the number of channels if each has a low p_{open} (Colquhoun and Hawkes, 1990).

Having established that the E166A and E166D mutations affect the fast gate, we next investigated the fast gate modification of E166D by pH_{int} and pH_{ext}. The fast gate of WT CLC-0 is known to be affected by pH but in a qualitatively different manner by pH_{int} and pH_{ext}. Changing pH_{int} mainly "shifts" the activation curve (Hanke and Miller, 1983), whereas lowering pH_{ext} mainly increases the "residual" p_{open} at negative voltages (Chen and Chen, 2001). The differential effect of internal and external pH on the open probability is related to the two possible routes by which the fast gate of CLC-0 can open (Chen and Miller, 1996). The opening rate constant shows a biphasic voltage dependence, rising both at negative as well as at positive voltages (Chen and Miller, 1996; Chen and Chen, 2001), however with different voltage dependencies. Extracellular protons increase the rate of opening favored at negative voltages and have no effect on the closing rate, whereas intracellular protons mostly seem to affect the closing rate (Hanke and Miller, 1983; Chen and Chen, 2001).

The molecular acceptor for intracellular protons is unknown. In contrast, it is believed that the increase of p_{open} of WT CLC-0 at low pH_{ext} is caused by a protonation of E166 and a consequent "unblocking" of the external Cl^- site, S_{ext} (Dutzler et al., 2003). Therefore, since p_{open} of the mutant E166D is so low we expected that decreasing pH_{ext} would dramatically increase currents over the whole voltage range by protonation of Asp166. Surprisingly, practically the only effect of lowering pH_{ext} was to increase the persistent current at negative voltages. Qualitatively, the effect of reducing pH_{ext} in WT CLC-0 and mutant E166D seems to be nevertheless very similar: steady inward currents are increased, whereas the "voltage-dependent part" of the p_{open}–voltage relationship is only slightly affected. There is, however, a significant difference. In WT CLC-0, single channel events that reflect the "persistent" conductance at negative voltages have the same conductance as the single channel events seen at more positive voltages. In contrast, in mutant E166D the persistent current is carried by a different, lower-conductance, open state. Several possibilities exist to explain this behavior. First, the persistent current of E166D could be mechanistically different from that in WT CLC-0. Even though we are not able to exclude this possibility, the similar pH_{ext} dependence and the relative voltage insensitivity suggest that these phenomena reflect the same molecular mechanism, i.e., opening of the channel by protonation of E166/D166 from the extracellular side. The major difficulty with this interpretation is that the conductance of this state in mutant E166D is ~10-fold smaller than the depolarization-induced open state.

Lowering pH_{int} dramatically increased currents carried by E166D. For pH_{int} values >5 we could describe the activation by a shift of the $p_{open}(V)$ curve along the voltage axis. At more acidic pH_{int} ($pH < 5$), a qualitatively new behavior appeared that was not followed further in detail. In particular, at very acidic pH_{int} inward

"tail" currents became very small, despite the large outward currents. Future studies are needed to characterize this interesting phenotype in more detail.

For $pH_{int} > 5$, the mechanism of action of intracellular protons seems to be similar to that of WT CLC-0, i.e., lowering pH_{int} "shifts" the $p_{open}(V)$ curve to more negative voltages. In contrast to WT CLC-0 the voltage of half-maximal activation was very positive (+74 mV) even at the lowest pH for which we were able to perform a Boltzmann analysis (5.3). Activation saturated at voltages ≥200 mV and pH_{int} ≤5.8, even if it is not entirely clear if the open probability approaches unity under these conditions. Assuming a saturating p_{open} of 1 allows estimation the absolute p_{open} for the conditions under which the single channel measurements were performed (pH 7.2, V = 80 mV). The value from these macroscopic measurements (0.95%) is in qualitative agreement with that obtained from the single-channel measurements (0.5%). However, the noisy appearance of the current traces at these saturating voltages suggests that the open probability was actually below unity, meaning that the value of 0.95% is an overestimation of the true open probability.

Hanke and Miller (1983) described the effect of pH_{int} on CLC-0 with a four-state model

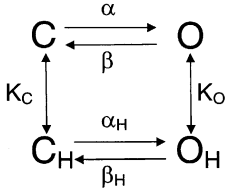

(MODEL 1)

in which unprotonated channels open and close with rate constants α and β, respectively, whereas protonated channels open and close with rate constants α_H and β_H, respectively. In the model, protonation of closed and open states occurs with binding constants K_C and K_O, respectively. Protonation favors opening if $\alpha_H/\beta_H > \alpha/\beta$. Assuming microscopic reversibility, Model 1 predicts the following dependence of the open probability on $[H] = [H]_{int}$:

$$p_{open} = p_O + p_{OH} = \frac{1 + [H]/K_O}{1 + \beta/\alpha + [H]/K_O + [H]/K_O * \beta_H/\alpha_H}. \quad (4)$$

Hanke and Miller (1983) concluded that most of the voltage dependence of opening should be attributed to the rate constants α and β (and α_H and β_H), whereas protonation and deprotonation, characterized by the constants K_O and K_C, was deduced to be almost voltage independent. The dependence of the voltage of half-maximal activation, $V_{1/2}$, on pH_{int} was thus described by the equation

$$V_{1/2} = \frac{-RT}{zF}\ln\left\{\frac{K_1(0)(1 + [H]/K_O)}{1 + [H]/K_C}\right\}, \quad (5)$$

where z is the apparent gating valence that describes the steepness of the voltage dependence of the open probability (Eq. 18 in Hanke and Miller, 1983). For the *Torpedo* channel, Hanke and Miller obtained a value for z ~1 (Hanke and Miller, 1983), whereas for E166D we found a slightly smaller value of z ~0.74 (Fig. 8, legend). $K_1(0)$ is the value of α/β at 0 mV. Eq. 5 predicts that $V_{1/2}$ levels off at low [H] and high [H] at values $-RT/zF*\ln(K_1(0))$ and $-RT/zF*\ln(K_1[0]*K_C/K_O)$, respectively. In contrast to this prediction of the model of Hanke and Miller (1983), no clear saturation of the $V_{1/2}$ values is seen for E166D at either low or high pH values (Fig. 8 B). Indeed, the data shown in Fig. 8 B can only be well fitted by Eq. 5 if the parameter z is adjusted to a value of 0.59, significantly smaller than the steepness of the $p_{open}(V)$ curve at pH 5.3 and pH 5.8 (dashed line in Fig. 8 B). Furthermore, the fit predicts that the pK of the hypothetical proton-accepting group must change from 12.2 in the closed state to 5.3 in the open state, a change by 7 log units. Such a huge change of pK is rather unlikely. A more consistent description of our data can be obtained if, in disagreement with the conclusion of Hanke and Miller (1983) it is assumed that the protonation/deprotonation reaction carries most of the voltage dependence, whereas the "conformational" rates α and β are less voltage dependent. Our data are not detailed enough to allow a precise determination of an exact model. We will thus consider only a simplified model in which opening occurs only for protonated channels. This simplification appears to be justified by the finding that the open probability of E166D in the absence of protons is extremely small.

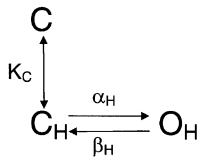

(MODEL 2)

Assuming that α_H and β_H are voltage independent, and that instead the protonation constant K_C depends exponentially on voltage

$$K_C = K_C(0)\exp(-zVF/RT), \quad (6)$$

Model 2 predicts

$$p_{open} = \frac{1}{1 + \beta_H/\alpha_H + \beta_H/\alpha_H * K_C/[H]} = \frac{\alpha_H}{\alpha_H + \beta_H}\frac{1}{1 + \exp\left(\frac{z(V_{1/2} - V)F}{RT}\right)} \quad (7)$$

with

$$V_{1/2} = \frac{RT}{zF}\ln\left\{\frac{\beta_H}{\alpha_H + \beta_H}\frac{K_C(0)}{[H]}\right\}, \quad (8)$$

and if $\beta_H/\alpha_H << 1$, the open probability follows practically a Boltzmann distribution. Most importantly, Eq. 8 predicts that the voltage of half maximal activation depends linearly on pH. This is indeed found for the mutant E166D (Fig. 8 B), and seems also to be an appropriate description of the data reported for CLC-0 (see Fig. 5 in Hanke and Miller, 1983). The argument Hanke and Miller used to conclude that protonation/deprotonation is voltage independent was that the apparent gating valence of the Boltzmann distribution describing the voltage dependence of p_{open} was independent of pH. However, also Eq. 7 predicts a constant gating valence even though the voltage dependence arises exclusively from protonation/deprotonation. Thus, also the data of Hanke and Miller (1983) may allow the alternative interpretation proposed here that at least part of the voltage dependence lies in the protonation step.

We found a change of $V_{1/2}$ of ~81 mV per pH unit (see solid line in Fig. 8 B) corresponding to a voltage dependence of ~0.71 elementary charges in Eq. 6, in good agreement with the observed steepness of the voltage dependence of the $p_{open}(V)$ curves ($z \sim 0.74$; Fig. 8, legend). In this simple model the steepness of the voltage dependence of the activation curve reflects mainly the voltage dependence of the protonation from the intracellular side.

The quantitative conclusions from the above considerations are limited by (at least two) factors. First, the data obtained for E166D are not ideal because the $p_{open}(V)$ curve does not saturate for the two more alkaline pH values shown in Fig. 8 B. Thus, the $V_{1/2}$ values for pH 7.2 and pH 6.8 shown in Fig. 8 B are relatively rough estimates. Unfortunately at more acidic pH values, for which better defined $V_{1/2}$ values might be expected to be definable, a qualitative new behavior of the mutant emerged, rendering impossible an analysis in terms of the usual open probability. Second, the Model 2 is certainly an oversimplification because the contribution of chloride ions to the voltage dependence of gating is completely neglected. Furthermore, the model does not consider the effect of extracellular protons on the open probability. Despite all these uncertainties, we believe that the idea that one of the major sources of voltage dependence of the gating of CLC-0 arises from a protonation step from the intracellular side is a viable hypothesis. The simple Model 2 assumes protonation directly from the intracellular solution. This seems to be unrealistic, however, if the target of protonation is the residue at position 166. In fact, it is more likely that protonation involves several intermediate proton acceptors that remain to be identified. It is also not clear whether protons from the intracellular side use the same pathway as permeating chloride ions.

Collectively, from our detailed analysis of the conservative mutant E166D, two principal speculations are suggested. First, a major voltage-dependent step of the activation of the fast gate results from a voltage-dependent protonation from the intracellular side. Second, and even more speculatively, protonation of the acidic residue at position 166 (E or D) from the outside and protonation from the inside leads to different open states that have a different single-channel conductance in mutant E166D. In WT CLC-0 these two open states have either a similar conductance or they immediately collapse into a common open state. In contrast, in the mutant E166D the two open states are clearly distinct and not simply interconvertable. In this respect it is noteworthy that a recent theoretical study proposed that the side chain of E166 can adopt an inwardly directed conformation, one that may be susceptible for accepting intracellular protons (Bisset et al., 2005). It will also be highly interesting to study the functional and structural effect of mutating the corresponding glutamate residue to aspartate in the bacterial CLC-ec1. The continuous feedback between functional and structural data will undoubtedly provide an ever better understanding of this unique class of ion channels and transporters.

We thank Laura Elia for expert technical assistance, Alessandra Picollo, and Elena Babini for suggestions on the manuscript, Giacomo Gaggero for help in constructing the perfusion system, and Enrico and Giacomo Gaggero for constructing the high impedance amplifier.

The financial support by Telethon Italy (grant GGP04018) and the Italian Research Ministry (FIRB RBAU01PJMS) is gratefully acknowledged. S. Traverso received a Consiglio Nazionale delle Ricerche doctoral fellowship.

David C. Gadsby served as editor.

Submitted: 31 May 2005
Accepted: 9 December 2005

REFERENCES

Accardi, A., and C. Miller. 2004. Secondary active transport mediated by a prokaryotic homologue of ClC Cl^- channels. *Nature.* 427:803–807.

Accardi, A., and M. Pusch. 2000. Fast and slow gating relaxations in the muscle chloride channel CLC-1. *J. Gen. Physiol.* 116:433–444.

Accardi, A., and M. Pusch. 2003. Conformational changes in the pore of CLC-0. *J. Gen. Physiol.* 122:277–293.

Accardi, A., L. Ferrera, and M. Pusch. 2001. Drastic reduction of the slow gate of human muscle chloride channel (ClC-1) by mutation C277S. *J. Physiol.* 534:745–752.

Bauer, C.K., K. Steinmeyer, J.R. Schwarz, and T.J. Jentsch. 1991. Completely functional double-barreled chloride channel expressed from a single *Torpedo* cDNA. *Proc. Natl. Acad. Sci. USA.* 88: 11052–11056.

Bisset, D., B. Corry, and S.H. Chung. 2005. The fast gating mecha-

nism in ClC-0 channels. *Biophys. J.* 89:179–186.

Chen, M.F., and T.Y. Chen. 2001. Different fast-gate regulation by external Cl^- and H^+ of the muscle-type ClC chloride channels. *J. Gen. Physiol.* 118:23–32.

Chen, T.Y., and C. Miller. 1996. Nonequilibrium gating and voltage dependence of the ClC-0 Cl^- channel. *J. Gen. Physiol.* 108:237–250.

Colquhoun, D., and A.G. Hawkes. 1990. Stochastic properties of ion channel openings and bursts in a membrane patch that contains two channels: evidence concerning the number of channels present when a record containing only single openings is observed. *Proc. R. Soc. Lond. B. Biol. Sci.* 240:453–477.

Dutzler, R., E.B. Campbell, M. Cadene, B.T. Chait, and R. MacKinnon. 2002. X-ray structure of a ClC chloride channel at 3.0 Å reveals the molecular basis of anion selectivity. *Nature.* 415:287–294.

Dutzler, R., E.B. Campbell, and R. MacKinnon. 2003. Gating the selectivity filter in ClC chloride channels. *Science.* 300:108–112.

Estévez, R., B.C. Schroeder, A. Accardi, T.J. Jentsch, and M. Pusch. 2003. Conservation of chloride channel structure revealed by an inhibitor binding site in ClC-1. *Neuron.* 38:47–59.

Fersht, A. 1998. Structure and Mechanism in Protein Science. WH Freeman and Company, New York. 631 pp.

Hanke, W., and C. Miller. 1983. Single chloride channels from *Torpedo* electroplax. Activation by protons. *J. Gen. Physiol.* 82:25–45.

Heinemann, S.H., and F. Conti. 1992. Nonstationary noise analysis and application to patch clamp recordings. *Methods Enzymol.* 207: 131–148.

Jentsch, T.J., K. Steinmeyer, and G. Schwarz. 1990. Primary structure of *Torpedo marmorata* chloride channel isolated by expression cloning in *Xenopus* oocytes. *Nature.* 348:510–514.

Jentsch, T.J., M. Poet, J.C. Fuhrmann, and A.A. Zdebik. 2005. Physiological functions of CLC Cl channels gleaned from human genetic disease and mouse models. *Annu. Rev. Physiol.* 67:779–807.

Lin, C.W., and T.Y. Chen. 2003. Probing the pore of ClC-0 by substituted cysteine accessibility method using methane thiosulfonate reagents. *J. Gen. Physiol.* 122:147–159.

Lin, Y.W., C.W. Lin, and T.Y. Chen. 1999. Elimination of the slow gating of ClC-0 chloride channel by a point mutation. *J. Gen. Physiol.* 114:1–12.

Lorenz, C., M. Pusch, and T.J. Jentsch. 1996. Heteromultimeric CLC chloride channels with novel properties. *Proc. Natl. Acad. Sci. USA.* 93:13362–13366.

Ludewig, U., M. Pusch, and T.J. Jentsch. 1996. Two physically distinct pores in the dimeric ClC-0 chloride channel. *Nature.* 383: 340–343.

Ludewig, U., T.J. Jentsch, and M. Pusch. 1997. Inward rectification in ClC-0 chloride channels caused by mutations in several protein regions. *J. Gen. Physiol.* 110:165–171.

Middleton, R.E., D.J. Pheasant, and C. Miller. 1996. Homodimeric architecture of a ClC-type chloride ion channel. *Nature.* 383:337–340.

Miller, C., and E.A. Richard. 1990. The voltage-dependent chloride channel of *Torpedo* electroplax. Intimations of molecular structure from quirks of single-channel function. *In* Chloride Channels and Carriers in Nerve, Muscle and Glial Cells. F.J. Alvarez-Leefmans and J.M. Russell, editors. Plenum, New York. 383–405.

Miller, C., and M.M. White. 1980. A voltage-dependent chloride conductance channel from *Torpedo* electroplax membrane. *Ann. NY Acad. Sci.* 341:534–551.

Miller, C., and M.M. White. 1984. Dimeric structure of single chloride channels from *Torpedo* electroplax. *Proc. Natl. Acad. Sci. USA.* 81:2772–2775.

Mindell, J.A., M. Maduke, C. Miller, and N. Grigorieff. 2001. Projection structure of a ClC-type chloride channel at 6.5 Å resolution. *Nature.* 409:219–223.

Picollo, A., and M. Pusch. 2005. Chloride/proton antiporter activity of mammalian CLC proteins ClC-4 and ClC-5. *Nature.* 436: 420–423.

Pusch, M., and T.J. Jentsch. 2005. Unique structure and function of chloride transporting CLC proteins. *IEEE Trans. Nanobioscience.* 4:49–57.

Pusch, M., K. Steinmeyer, and T.J. Jentsch. 1994. Low single channel conductance of the major skeletal muscle chloride channel, ClC-1. *Biophys. J.* 66:149–152.

Pusch, M., U. Ludewig, and T.J. Jentsch. 1997. Temperature dependence of fast and slow gating relaxations of ClC-0 chloride channels. *J. Gen. Physiol.* 109:105–116.

Pusch, M., A. Liantonio, L. Bertorello, A. Accardi, A. De Luca, S. Pierno, V. Tortorella, and D.C. Camerino. 2000. Pharmacological characterization of chloride channels belonging to the ClC family by the use of chiral clofibric acid derivatives. *Mol. Pharmacol.* 58:498–507.

Rychkov, G.Y., M. Pusch, D.S. Astill, M.L. Roberts, T.J. Jentsch, and A.H. Bretag. 1996. Concentration and pH dependence of skeletal muscle chloride channel ClC- 1. *J. Physiol.* 497:423–435.

Scheel, O., A.A. Zdebik, S. Lourdel, and T.J. Jentsch. 2005. Voltage-dependent electrogenic chloride/proton exchange by endosomal CLC proteins. *Nature.* 436:424–427.

Traverso, S., L. Elia, and M. Pusch. 2003. Gating competence of constitutively open CLC-0 mutants revealed by the interaction with a small organic inhibitor. *J. Gen. Physiol.* 122:295–306.

Uchida, S., and S. Sasaki. 2005. Function of chloride channels in the kidney. *Annu. Rev. Physiol.* 67:759–778.

White, M.M., and C. Miller. 1979. A voltage-gated anion channel from the electric organ of *Torpedo californica. J. Biol. Chem.* 254: 10161–10166.